AD-A130 972 MATRIX CALIBRATION FOR THE QUANTITATIVE ANALYSIS OF LAYERED SEMICONDUCTOR..(U) CORNELL UNIV ITHACA NY DEPT OF CHEMISTRY A A GALUSKA ET AL. 27 JUL 83 TR-10 1/1

UNCLASSIFIED N00014-80-C-0538 F/G 20/12 NL

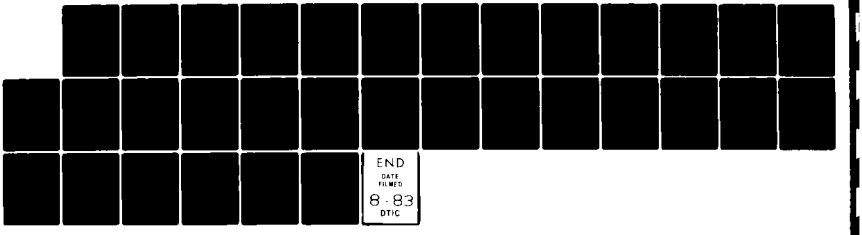

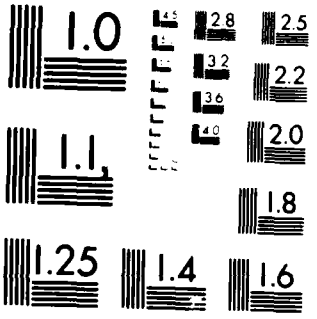

(12)

OFFICE OF NAVAL RESEARCH

Contract N0014-80-C-0538

Task No. NR 051-736

TECHNICAL REPORT NO. 11

MATRIX CALIBRATION FOR THE QUANTITATIVE ANALYSIS OF LAYERED SEMICONDUCTORS BY SECONDARY ION MASS SPECTROMETRY

by

Alan A. Galuska

George H. Morrison*

Prepared for Publication

in

Analytical Chemistry

Cornell University
Department of Chemistry
Ithaca, N. Y. 14853

July 27, 1983

REPORT DOCUMENTATION PAGE

READ INSTRUCTIONS BEFORE COMPLETING FORM

1. REPORT NUMBER	2. GOVT ACCESSION NO.	3. RECIPIENT'S CATALOG NUMBER
Technical Report No. 10	A130 972	

4. TITLE (and Subtitle)
MATRIX CALIBRATION FOR THE QUANTITATIVE ANALYSIS OF LAYERED SEMICONDUCTORS BY SECONDARY ION MASS SPECTROMETRY

5. TYPE OF REPORT & PERIOD COVERED
Interim Technical Report

6. PERFORMING ORG. REPORT NUMBER

7. AUTHOR(s)
A. A. Galuska and G. H. Morrison

8. CONTRACT OR GRANT NUMBER(s)
N00014-80-C-0538

9. PERFORMING ORGANIZATION NAME AND ADDRESS
Department of Chemistry
Cornell University, Ithaca, N. Y. 14853

10. PROGRAM ELEMENT, PROJECT, TASK AREA & WORK UNIT NUMBERS
NR051-736

11. CONTROLLING OFFICE NAME AND ADDRESS
ONR (472)
800 N. Quincy St., Arlington, VA 22217

12. REPORT DATE
July 27, 1983

13. NUMBER OF PAGES
28 pages

14. MONITORING AGENCY NAME & ADDRESS(if different from Controlling Office)

15. SECURITY CLASS. (of this report)
unclassified

15a. DECLASSIFICATION/DOWNGRADING SCHEDULE

16. DISTRIBUTION STATEMENT (of this Report)
Approved for public release: distribution unlimited

17. DISTRIBUTION STATEMENT (of the abstract entered in Block 20, if different from Report)

18. SUPPLEMENTARY NOTES
Prepared for publication in ANALYTICAL CHEMISTRY

19. KEY WORDS (Continue on reverse side if necessary and identify by block number)
SIMS, superlattice, multilayer-multimatrix samples, matrix effect calibration, practical ion yields, relative sensitivity factor, relative ion yields, $Al_xGa_{1-x}As$, molecular beam epitaxy, ion implantation, relative sputtering yields

20. ABSTRACT (Continue on reverse side if necessary and identify by block number)
Analyses of $Al_xGa_{1-x}As$ matrices by secondary ion mass spectrometry (SIMS) have shown that secondary ion yields and sputtering yields are linearly dependent on the sample composition. Calibration lines for Be, Si, B, P, and As were obtained using practical ion yields, relative sensitivity factors, and relative ion yields. Calibration lines formed using relative ion yields provided superior precision and accuracy. Relative ion yield and relative sputtering yield calibration lines were applied to the determination of a $^{11}B^+$ implant into a multilayer-multimatrix sample.

DD FORM 1 JAN 73 1473

SECURITY CLASSIFICATION OF THIS PAGE (When Data Entered)

MATRIX CALIBRATION FOR THE QUANTITATIVE ANALYSIS OF LAYERED SEMICONDUCTORS BY SECONDARY ION MASS SPECTROMETRY

A. A. Galuska and G. H. Morrison*

Department of Chemistry
Cornell University
Ithaca, New York 14853

BRIEF

The linearity of secondary ion yields and sputtering yields with composition was shown for $Al_xGa_{1-x}As$. Calibration lines for Be, Si, B, P, and As were obtained using practical ion yields, relative sensitivity factors and relative ion yields.

AC8303825

The sputtering and ionization of surface atoms by ion bombardment is the basis of secondary ion mass spectrometry (SIMS). High sensitivity for most elements and excellent depth resolution (less than 100 Å) have made SIMS an attractive method for concentration depth profiling. Although the technique had been applied successfully to a variety of materials, the complexity of the sputtering event has made quantitative analysis difficult. Secondary ion yields vary over several orders of magnitude. In addition, the ion yield of each element is influenced by a variety of factors including the nature of the primary ion beam (1-3), residual gas pressure (4), and matrix effects (5, 6).

The fabrication of external and internal standards by ion implantation has provided an accurate (± 15%) means of quantifying trace element distributions in homogeneous matrices (7-9). However, due to varying matrix effects, the quantitative analysis of heterogeneous matrices is extremely difficult. A depth profile of a sample composed of more than one matrix (in particular, layers of different matrices stacked one on top of the other) becomes distorted by the variation of secondary ion yields and sputtering yields with matrix: signal and time are no longer proportional to concentration and depth, respectively.

There are two principal explanations for the variation of secondary ion yields with matrix. It has been suggested that matrix effects are merely a function of sputtering yield (10, 11). Lower

sputtering yields enhance the build-up of reactive primary ions (O^+ or Cs^+) in surface layers resulting in increased secondary ion yields. Alternatively, others (12, 13) have asserted that ion yields are a linear function of matrix composition. Neither theory attempts to explain the variation of sputtering yields with matrix. Neither theory has been rigorously evaluated or applied.

Current trends in semiconductor technology require the development of an applicable method of matrix calibration. Devices composed of Group III and V compound semiconductors (such as FET's, CW lasers, power FET's, IMPATT diodes, varactor diodes, and mixer diodes) are being rapidly developed (14-16) using growth techniques such as molecular beam epitaxy (MBE). These compound matrices are also being used to construct superlattices, alternating thin semiconductor layers of varying composition, Figure 1. There is a need for trace and major element quantification in and through these layers. The use of SIMS to monitor elemental distributions through thin layers and interfaces of varying composition is extremely difficult due to the changing matrix effects which are encountered. Proper calibration of ion yields and sputtering yields, however, can make quantitative concentration and depth measurements possible for these samples.

In this investigation, $Al_xGa_{1-x}As$ matrices grown by MBE and subsequently doped by ion implantation were examined for possible matrix calibration. Secondary ion yields and sputtering yields were found to be linear function of matrix composition. Calibrations using

practical ion yields, relative sensitivity factors, and relative ion yields were compared for precision and accuracy. The relative ion yield calibrations were precise and accurate to within 15%. Similarly, relative sputtering yield calibrations were precise and accurate to within 10%. The quantitative analysis of an $^{11}B^+$ implant into a multilayer-multimatrix sample was performed using relative sputtering yield and relative ion yield calibrations to correct the depth and concentration scales respectively.

EXPERIMENTAL

Sample Preparation. The $Al_xGa_{1-x}As$ matrices were layers grown by MBE on semi-insulating GaAs substrates. The value of x was varied from 0 to 0.37 while the total atomic density remained at 4.43×10^{22} atom/cm^3 ± 0.5%. The composition of the layers was determined by photoluminescence spectroscopy and verified to an accuracy of better than 10% (17) using Rutherford backscattering spectroscopy (RBS). Prior to implantation all samples were cleaned with acetone and methanol. A small piece of each sample was then mounted on an aluminum disk, using silver paint, for ion implantation. A set of samples was implanted with $^9Be^+$ and $^{28}Si^+$, and a second set was implanted with $^{11}B^+$ and $^{31}P^+$.

Instrumentation. $Al_xGa_{1-x}As$ layers waere grown in a VARIAN MBE-360 machine (18). RBS measurements were carried out on a GENERAL IONEX Tandetron Model 4110A. Analyses were performed using a 2.5 MeV He^+ ion beam and solid state detection at a 170° angle from the incident beam path. Ion implantation was performed using two different ion implanters. Each was equipped with a hot filament ion source, a magnet for mass separation, and quadrupoles for ion beam focusing. Table I lists the implantation parameters.

SIMS analysis was carried out with a CAMECA IMS-3f ion microanalyzer using an electron multiplier in the pulse counting mode for signal detection (19). The instrument is interfaced to a HEWLETT PACKARD 9845T microcomputer for control and data acquisition. A 1.0 μA O_2^+ primary beam was rastered over a 400 x 400 μm area at an energy of 5.5 KeV. The signal area was apertured down to a circle 60 μm in diameter, and positive secondary ions were monitored. All analyses were performed with a residual pressure of 2×10^{-8} torr, and an energy window of 130 eV. A multiple sample holder allowed several samples to be mounted simultaneously. The depths of the sputtered craters were measured using a TALYSTEP stylus device with a resolution of 50 Å.

Software. Programs for instrumental control, data analysis, and matrix correction were written in BASIC for the HP 9845T. Data collection was performed using five second integrations per mass for each point during the depth profiles.

Procedure. Following ion implantation, samples were depth profiled in groups of four using a multiple sample holder. Groups of samples, including in each case GaAs, were inserted simultaneously to insure near identical analysis conditions. After allowing the pressure in the sample chamber to reach a steady-state condition, the primary beam was focused to a spot of about 100 μm in diameter, and the proper mass settings were determined. Without manipulating any instrumental parameters, the samples were analyzed consecutively until at least three profiles of each sample had been completed. In addition to the implants, $^{75}As^{+}$ was monitored for matrix quantification.

RESULTS AND DISCUSSION

Data Analysis. After profiling the samples, there are several ways in which practical ion yields (τ) can be calculated (8). In this study, elemental sensitivity was assumed constant throughout the full range of the implants. The secondary ion signals were integrated, and the background signals subtracted. Practical ion yields were then obtained using the implant fluences F (atom/cm^2), integrated signals I (total counts), average atomic concentration C (atom/cm^3), and the area A (cm^2) and depth D (cm) of analysis:

$$\tau_{implant} = \text{ions/atoms} \cdot k_i = I_i / F_i \cdot A \qquad (1)$$

$$\tau_{matrix} = \text{ions/atoms} \cdot k_m = I_m / C_m \cdot A \cdot D \qquad (2)$$

where k_i and k_m are dimensionless instrumental factors representing the probability of detecting ions from the implant and matrix respectively. τ's however can change drastically between analyses. Secondary ion collection and instrumental transmission are influenced by operator adjustment and indeterminate instrumental fluctuations which occur during routine operation. To reduce this effect, it is common practice to use relative sensitivity factors (RSF), as given by Eqs. (3) and (4), in which the τ of an analyte is ratioed to that of a reference element of in the same matrix. A knowledge of the average concentration of the reference element (C_{ref}) over the range of the analysis is required.

$$RSF_{implant} = \tau_i \cdot k_{ref} / \tau_{ref} \cdot k_i = I_i \cdot C_{ref} \cdot D / F_i \cdot I_{ref} \qquad (3)$$

$$RSF_{matrix} = \tau_m \cdot k_{ref} / \tau_{ref} \cdot k_m = I_m \cdot C_{ref} / C_m \cdot I_{ref} \qquad (4)$$

The normalization procedure is designed to minimize the influence of instrumental variations.

In addition to τ's and RSF's, relative ion yields (Rτ) were also examined. Rτ's are defined, for these analyses, as the ratio of the ion yield (τ_x) of an element in the sample matrix ($Al_xGa_{1-x}As$) to the ion yield (τ_0) of the element in a standard matrix (GaAs) when both measurements are performed under identical analysis conditions. The Rτ's for implant and matrix elements are given by Eqs. (5) and (6) respectively.

$$R\tau_{implant} = \tau_x/\tau_0 = I_x/I_0 \qquad (5)$$

$$R\tau_{matrix} = \tau_x/\tau_0 = I_x \cdot C_0 \cdot D_0 / I_0 \cdot C_x \cdot D_x \qquad (6)$$

Like RSF's, Rτ's are designed to minimize the influence of instrumental variations. However, Rτ's have several advantages over RSF's for matrix calibration. First, Rτ's do not mask ion yield information the way RSF's can: Rτ's are directly proportional to individual ion yields while RSF's are related to the ion yields of both the analyte and the reference elements. Moreover, since the instrumental factors of the analyte and the reference (k_a and k_{ref}) can vary independently, RSF's are influenced by instrumental variations to a greater extent than the Rτ's. In addition, Rτ's are

designed to normalize matrix effects while RSF's are not.

In addition to ion yields, sputtering yields were also examined as a function of matrix composition. Sputtering yields (S) are defined in terms of the erosion rate $\dot{z}^{\circ}$ (cm/sec), atomic density of the sample N (atom/cm^3), and the primary-ion current density J (ions/cm^2-sec).

$$S = \text{secondary atoms/primary atoms} = \dot{z}^{\circ} \cdot N/J \qquad (7)$$

However, measurements of S are inconvenient due to the imprecision with which J is measured. To overcome this difficulty, the sputtering yields of the sample matrices ($Al_xGa_{1-x}As$) have been normalized to the sputtering yields of the standard matrix (GaAs) measured under near identical conditions. Assuming J does not change between analyses, these relative sputtering yields (RS) take a simple form.

$$RS = S_x/S_0 = \dot{z}^{\circ}_x \cdot N_x/\dot{z}^{\circ}_0 \cdot N_0 \qquad (8)$$

Since the atomic density of $Al_xGa_{1-x}As$ does not change substantially with x, Eq. (8) can be reduced to a ratio of erosion rates for these matrices. Consequently, relative sputtering yields provide a means of

determining the erosion rates of sample matrices regardless of current density.

Precision and Accuracy. If ion yields are linearly dependent on matrtix composition, the practical ion yield of an element g (τ^g) can be described in the following manner (12):

$$\tau^g \propto \sum_{i=1}^{n} P_i^g \cdot C_i \qquad (9)$$

where n and C_i represent the total number of sample elements and the atomic concentration ($atom/cm^3$) of element i, respectively. P_i^g is a dimensionless quantity representing the influence of element i on the ion yield of element g. Ignoring the effect of trace elements (elements of less than one atomic percent), Eq. (9) takes the following form for $Al_xGa_{1-x}As$:

$$\tau^g \propto (P_{Al}^g - P_{Ga}^g) \cdot x + P_{Ga}^g + P_{As}^g. \qquad (10)$$

According to Eq. (10), a plot of τ, RSF, or Rτ versus x should yield a straight line.

Tables II, III, and IV summarize the results obtained using τ,

RSF, and Rτ respectively. Each calibration is characterized by the date of analysis, standards used, y-intercept, slope, linear correlation, relative standard deviation of the slope, and the average relative standard deviation of a single point. In addition, analyses performed on different weeks were combined to form total calibrations. These total calibrations are useful to determine the precision of the calibration lines and the precision of individual points from week to week.

The quality of these calibration procedures can be evaluated in terms of the precision of the line, and the precision of each point. The Rτ calibrations have excellent linearity followed by the τ calibrations, and then the RSF calibrations. Similarly, the relative standard deviations of the slopes are smallest (≃ 9%) when Rτ's are being used. In addition, the Rτ calibration lines are reproducible from week to week while the τ and RSF lines are not. The poorer precision of the τ calibration lines can be attributed to the poor reproducibility of individual τ measurements. The inferior quality of the RSF calibrations lines indicates that the ion yields of the analyte and the reference elements are not influenced proportionally by the matrix and instrumental effects which are encountered. Consequently, RSF's are not suitable for this type of calibration. Alternatively, Rτ's are well suited to matrix calibration.

The quality of a calibration procedure can also be judged by the precision of each measurement. When measurements are limited to a

single analysis period, Rτ's and RSF's give similar precisions (7% and 10% respectively) while τ's are less precise (18%). However, when measurements are performed on different weeks, Rτ's maintain good precision (9%) while the precision of the RSF's (24%) and τ's (60%) deteriorates. The precision of RSF's is limited by those factors that influence the analyte and reference differently. Alternatively, the precision of Rτ's is limited by the differences in the conditions under which the standard matrix and the sample matrix are analyzed. The limitations on the precision of the Rτ's are more efficiently minimized than those of the RSF's. Overall, the Rτ calibrations provide superior linearity and precision. Moreover, preliminary analysis indicates that an accuracy of 15% can generally be obtained using Rτ calibrations.

In addition to relative ion yields, relative sputtering yields were also monitored as a function of matrix composition. As shown in Table V, the relationship is linear. The lines are quite precise and reproducible from week to week. Moreover, these RS calibration lines have been used to determine the erosion rates of $Al_xGa_{1-x}As$ matrices with an accuracy of better than 10%. Using RS calibrations to determine erosion rates and Rτ calibrations to determine concentrations, it is now possible to quantitatively analyze multilayer-multimatrix samples.

Application. The use of Rτ and RS calibration lines for quantitative analysis is straight forward. The concentration of

analyte at each point of a depth profile C_p (atom/cm^3) can be determined using Eq. (11).

$$C_p = I_p/R\tau_x \cdot \tau_0 \cdot D_p \cdot A \qquad (11)$$

$R\tau_x$ is the relative sputtering yield determined from a calibration line for the appropriate value of x, and τ_0 is the practical ion yield of the analyte in the standard matrix (GaAs). I_p is the signal and D_p is the depth increment associated with each point of the depth profile. Similarly, the erosion rate at each point of a depth profile $\dot{z}_p$ can be determined using Eq. (12).

$$\dot{z}_p = RS_x \cdot \dot{z}_0 \cdot N_0/N_x \qquad (12)$$

RS_x is the relative sputtering yield determined from a calibration line for the appropriate value of x, and $\dot{z}_0$ is the sputtering rate of the standard matrix (GaAs). N_0 and N_x are the atomic densities of the standard matrix and the sample respectively. These calibrations may be used to analyze both homogeneous and multilayer-multimatrix samples.

Since these calibration lines are reproducible from week to week,

they are quite convenient for the quantitative analysis of homogeneous matrices. There are however two requirements. The sample and the standard matrices must be analyzed under identical conditions; consequently, a multiple sample holder is desireable. In addition, the matrix composition must be determined. This composition can be evaluated prior to SIMS analysis using a nondestructive technique such as RBS or photoluminescence. Alternatively, one may evaluate the matrix composition during the SIMS analysis. Since the concentration of As is constant for $Al_xGa_{1-x}As$ matrices, the slope of the As calibration line and the $R\tau$ of As determined from the sample can be used to obtain the value of x.

$$x = (R\tau - 1)/slope \qquad (13)$$

The accuracy of the SIMS and RBS measurements are comparable (15% and 10% respectively).

A multilayer-multimatrix sample can be quantitatively analyzed as a series of homogeneous matrices. Each layer may be treated as a homogeneous matrix. In addition, the interfaces, in which the composition changes from one matrix to another, can be approximated by linear concentration gradients. Alternatively, one may also treat each point of a depth profile as a homogeneous matrix by performing a point-by-point matrix calibration (A detailed description of this

process will be presented in a future paper.).

A 250 KeV $^{11}B^+$ implant into a layered sample ($GaAs/Al_{.12}Ga_{.88}As/GaAs$) provides a good example for the correction of matrix effects. In Figure 2a, the uncorrected SIMS depth profile of $^{11}B^+$ (dashed line) and $^{75}As^+$ (solid line) in this sample is presented. The first interface occurs at 33 time units while the second interface has not been reached in this profile. Due to matrix effects, the vertical and horizontal scales are no longer linearly related to concentration and depth, respectively. The peak in the $^{11}B^+$ profile at 34 time units is an excellent example of a distortion introduce by the changing matrix effects at the interface. In Figure 2b, the horizontal scale has been transformed into depth using Eq. (12), and the concentration of AL (solid line) at each point has been calculated from the $^{75}As^+$ profile using Eq. (13). The $^{11}B^+$ profile was then corrected and quantified using Eq. (11). An Al concentration of 2.4 X 10^{21} atom/cm^3 ± 6.0% was calculated for the $Al_xGa_{1-x}As$ layer which agrees to within experimental error with the value obtained from the RBS analysis (2.7 X 10^{21} atom/cm^3). The correction procedure had also removed the distorted interface region of the $^{11}B^+$ profile, transforming the profile into the expected gaussian shape. Thus, the application of this correction procedure can make a tremendous difference in the evaluation of SIMS profiles through layered multimatrix structures.

ACKNOWLEDGMENT

The authors gratefully acknowledge the assistance of C. Palmstrom and J. Mayer with the RBS measurements, and B. Shaft for the growth of the MBE matrices. Also acknowledged is the help of H. Dietrich of the Naval Research Laboratories (NRL) for his assistance with the ion implants. The ion implants were performed at both NRL and the National Research and Resource Facility for Submicron Structures at Cornell.

CREDIT

This work was supported by the National Science Foundation and the Office of Naval Research.

LITERATURE CITED

(1) Ishitani, T.; Tamara, H.; Shinmiyo, T. Surf. Sci. 1976, 55, 179-188.

(2) Storms, H. A.; Brown, K. F.; Stein, J. D. Anal. Chem. 1977, 49, 2023-2030.

(3) Barcz, A.; Domanski, M.; Woitowicz-Natanson, B. "Secondary Ion Mass Spectrometry SIMS III"; Benninghoven, A.; Giber, J.; Riedel, M.;Werner, H. W., Eds.; Springer-Verlag: New York, 1981, 134-139.

(4) Morgan, A. E.; Werner, H. W. Anal. Chem. 1976, 48, 699-708.

(5) McCracken, G. M. Rep. Prog. Phys. 1975, 38, 241-327.

(6) Blaise, G.; Bernheim, M. Surf. Sci. 1975, 47, 324-343.

(7) Gries, W. H. Int. J. Mass Spectrum. Ion Phys. 1979, 30, 97-112.

(8) Leta, D. P.; Morrison, G. H. Anal. Chem. 1980, 52, 514-519.

(9) Leta, D. P.; Morrison, G. H. Anal. Chem. 1980, 52, 277-280.

(10) Deline, V. R.; Katz, W.; Evans, C. A.; Williams, P. Appl. Phys. Lett. 1978, 33, 832-834.

(11) Deline, V. R.; Evans, C. A.; Williams, P. Appl. Phys. Lett. 1978, 33, 578-580.

(12) Slodzian, G. "Secondary Ion Mass Spectrometry SIMS III"; Benninghoven, A.; Giber, J.; Laszlo, J.; Riedel, M.; Werner, H. W., Eds.; Springer-Verlag: New York, 1981, pp 115-123.

(13) Steele, I.; Herrig, R.; Hutcheon, I. Proceedings of the 15th Annual Conference of the Microbeam Analysis Society, San Francisco, CA, 1980, pp 151-153.

(14) Panish, M. B. Science 1980, 20, 916-922.

(15) Cho, A. Y.; Arthur, J. R. "Progress in Solid State Chemistry"; Somorgai, G.; McCaldin, J., Eds.; Pergamon: New York, 1975; Vol. 10, pp 157-191.

(16) Cho, A. Y. J. Vac. Sci. Technol. 1979, 16, 275-284.

(17) Mayer, J. W.; Ziegler, J. F.; Chang, L. L.; Tsu, R.; Esaki, L. J. Appl. Phys. 1973, 44, 2322-2325.

(18) Daries, G. J.; Heckingbottom, R.; Ohno, H.; Wood, C. E. C.; Calawa, A. R. Appl. Phys. Lett. 1980, 37, 290-292.

(19) Ruberol, J. M.; Lepareur, M.; Autier, B.; Gourgout, J. M. VIIIth International Congress on X-ray Optics and Microanalysis and 12th Annual Conference of the Microbeam Analysis Society, Boston, MA, 1977, pp 133A-133D.

Table I. Implantation Parameters

Implant Element	$Al_xGa_{1-x}As$ Matrix (x)	Fluence ($atom/cm^2$)	Energy (KeV)	Source
^{9}Be	0-0.37	1×10^{14}	250	Be solid
^{11}B	0-0.37	1×10^{14}	250	BF_3 gas
^{28}Si	0-0.37	1×10^{15}	250	SiF_4 gas
^{31}P	0-0.37	1×10^{15}	300	PF_3 gas

Table II. Practical Ion Yield Calibrations for $Al_xGa_{1-x}As$ Matrices

Analyte	Week No.	X Values	Intercept X 10^{-7}	Slope X 10^{-5}	Linear Correlation r^2	RSD Slope %
^{9}Be	1	0,.12,.26,.37	1.23	41.5	0.927	32.8
	2	0,.13,.21,.37	116	67.3	0.915	68.6
	3	0,.13,.18,.21	61.4	32.3	0.995	9.5
^{28}Si	1		36.4	22.2	0.989	18.5
	2		25.3	15.2	0.987	17.0
	3		38.9	17.7	0.984	10.8
^{31}P	16	0,.18,.26,.31	0.822	0.291	0.936	18.6
	32	0,.13,.18,.37	1.17	0.258	1.000	2.0
^{11}B	16		25.8	7.05	0.734	53.6
	32		28.2	17.0	0.994	8.7
^{75}As	1		1.78	0.130	0.966	14.6
	2		0.932	0.0891	0.915	21.0
	3		0.940	0.108	0.984	11.0
	32		0.918	0.0532	0.932	11.2
		Avg RSD per point = 18.4%				
^{9}Be	Total		31.4	44.7	0.868	12.3
^{28}Si	Total		11.0	19.0	0.994	5.8
^{31}P	Total		1.00	0.278	0.928	12.4
^{11}B	Total		27.0	15.3	0.825	18.8
^{75}As	Total		0.642	0.111	0.722	19.2
		Avg RSD per point = 60.4%				

Table III. Relative Sensitivity Factor Calibrations for $Al_xGa_{1-x}As$ Matrices

Analyte Reference	Week No.	X Values	Intercept	Slope	Linear Correlation r^2	RSD Slope %
$^{9}Be/^{75}As$	1	0,.12,.26,.37	47.0	890	0.731	33.6
	2	0,.13,.21,.37	84.8	573	0.894	23.0
	3	0,.13,.18,.21	66.5	950	0.995	4.7
$^{28}Si/^{75}As$	1		39.8	271	0.708	38.2
	2		39.4	382	0.903	24.2
	3		36.0	711	0.936	37.8
$^{31}P/^{75}As$	16	0,.18,.26,.31	1.58	9.67	0.715	40.3
	32	0,.13,.18,.37	1.88	4.91	0.827	58.9
$^{11}B/^{75}As$	16		30.7	454	0.945	26.1
	32		60.9	509	0.940	17.1
		Avg RSD per point = 10.4%				
$^{9}Be/^{75}As$	Total		88.7	740	0.694	16.8
$^{28}Si/^{75}As$	Total		42.7	357	0.804	17.7
$^{31}P/^{75}As$	Total		2.41	4.45	0.464	79.2
$^{11}B/^{75}As$	Total		34.0	481	0.883	19.2
		Avg RSD per point = 24.4%				

Table IV. Relative Ion Yield Calibrations for $Al_xGa_{1-x}As$ Matrices

Analyte	Week No.	X Values	Intercept	Slope	Linear Correlation r^2	RSD Slope %
^{9}Be	1	0,.12,.26,.37	1.0	52.9	0.999	6.4
	2	0,.13,.21,.37	1.0	42.6	0.996	4.3
	3	0,.13,.18,.21	1.0	41.7	1.000	14.2
^{28}Si	1		1.0	44.5	1.000	9.8
	2		1.0	40.1	0.975	5.7
	3		1.0	45.9	1.000	9.6
^{31}P	16	0,.18,.26,.31	1.0	21.2	0.995	9.6
	32	0,.13,.18,.37	1.0	23.0	1.000	2.5
^{11}B	16		1.0	46.7	0.990	10.7
	32		1.0	39.5	1.000	8.6
^{75}As	1		1.0	6.00	0.933	15.7
	2		1.0	6.54	0.991	2.8
	3		1.0	5.76	0.980	12.4
	32		1.0	5.32	0.925	11.0
		Avg RSD per point = 7.4%				
^{9}Be	Total		1.0	46.3	0.981	13.7
^{28}Si	Total		1.0	44.7	0.986	5.0
^{31}P	Total		1.0	22.1	0.942	4.6
^{11}B	Total		1.0	46.6	0.961	7.0
^{75}As	Total		1.0	5.76	0.917	7.0
		Avg RSD per point = 9.2%				

Table V. Relative Sputtering Yield Calibrations for $Al_xGa_{1-x}As$ Matrices

Week No.	Intercept	Slope	Linear Correlation r^2	RSD Slope %
1	1.0	-1.00	0.928	11.8
2	1.0	-1.01	0.913	12.5
3	1.0	-0.89	0.991	4.0
16	1.0	-0.88	0.997	3.2
32	1.0	-0.75	0.934	11.6
	Avg RSD per point = 3.8%			
Total	1.0	-0.86	0.906	8.3
	Avg RSD per point = 7.9%			

FIGURE CAPTIONS

Figure 1. A hypothetical $Al_xGa_{1-x}As$ superlattice. The thickness T of the layers can vary from several angstroms to several microns while x can be varied from 0 to 1.

Figure 2. SIMS depth profile of a 250 Kev $^{11}B^+$ implant into a $GaAs/Al_{0.12}Ga_{0.88}As/GaAs$ sample. (a) uncorrected profile of $^{11}B^+$ (- - -) and $^{75}As^+$ (——); (b) concentration profiles of B (- - -) {2.0 X 10^{18} atom/cm^3 full scale } and Al (——) {1.0 X 10^{22} atom/cm^3 full scale}.

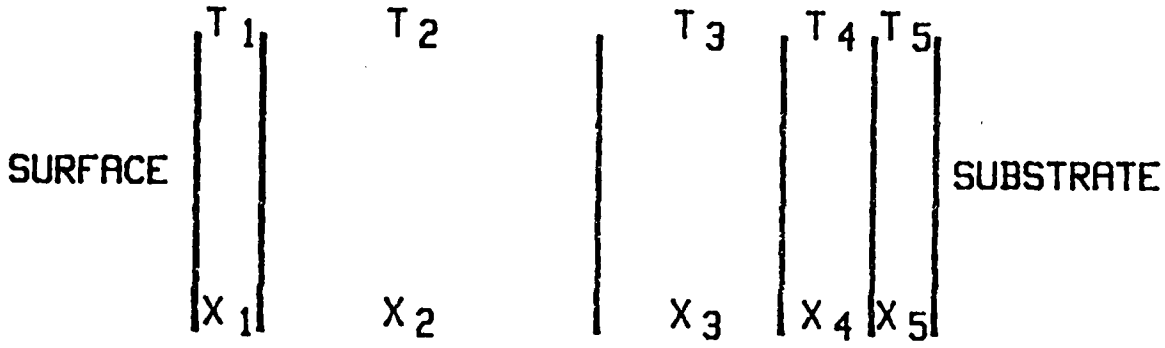
T 1
T 2
T 3
T 4
T 5
SURFACE
SUBSTRATE
X 1
X 2
X 3
X 4
X 5

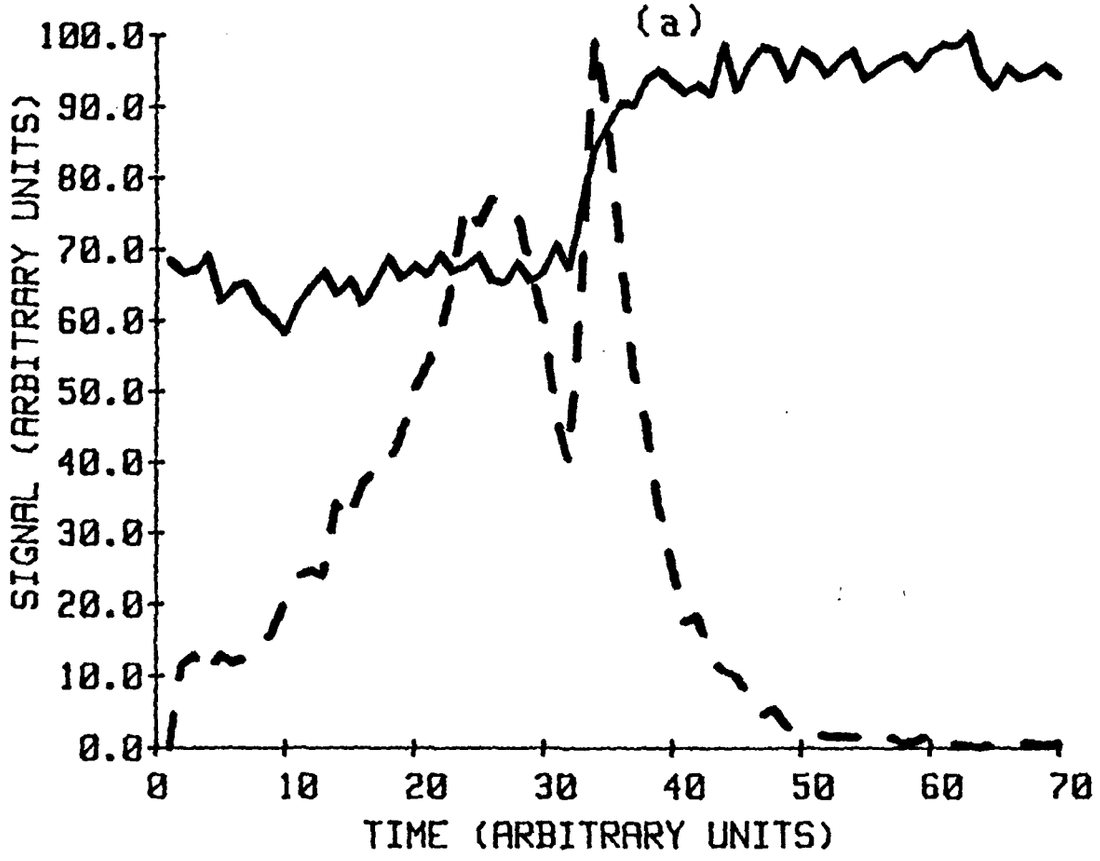
(a)
100.0
90.0
80.0
70.0
60.0
50.0
40.0
30.0
20.0
10.0
0.0
SIGNAL (ARBITRARY UNITS)
0
10
20
30
40
50
60
70
TIME (ARBITRARY UNITS)

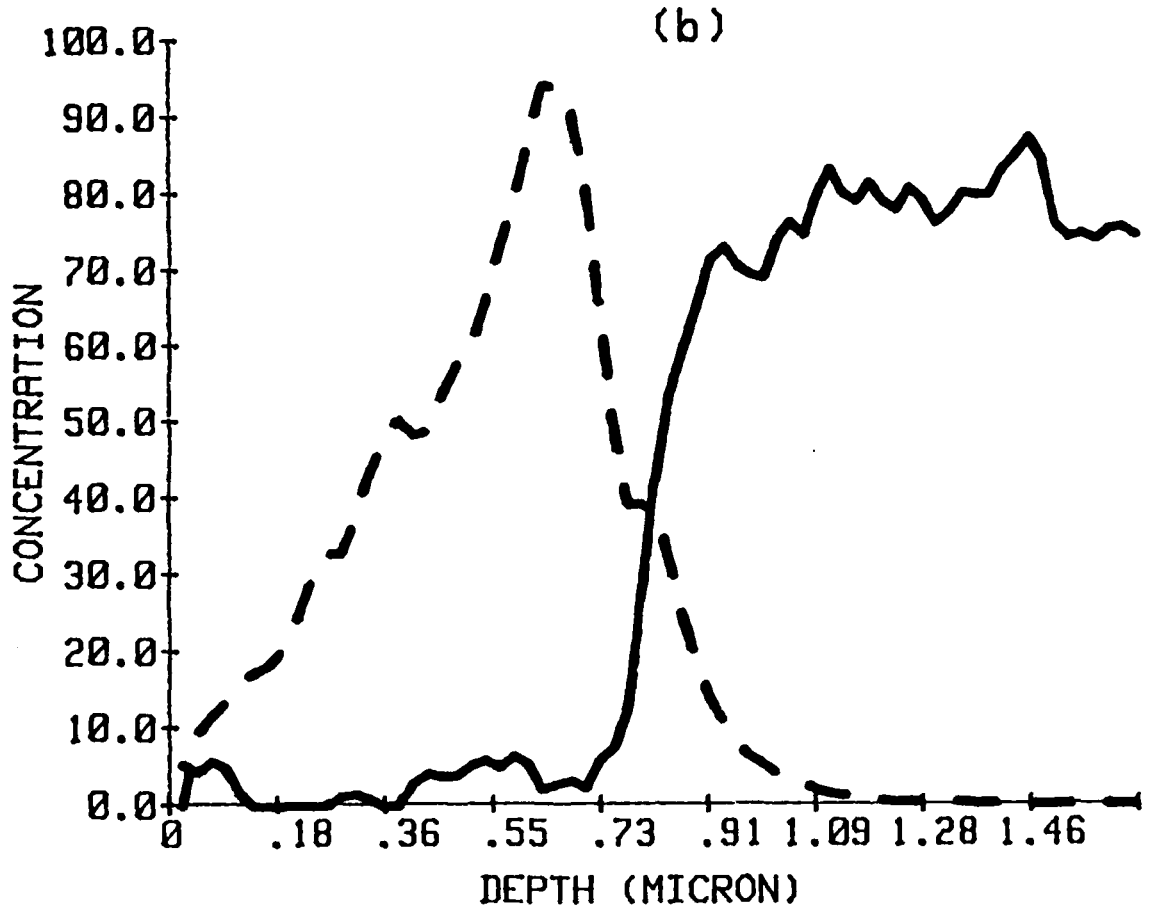
(b)
100.0
90.0
80.0
70.0
60.0
50.0
40.0
30.0
20.0
10.0
0.0
CONCENTRATION
0
.18
.36
.55
.73
.91
1.09
1.28
1.46
DEPTH (MICRON)

TECHNICAL REPORT DISTRIBUTION LIST, 359

	No. Copies
Office of Naval Research Attn: Code 472 800 North Quincy Street Arlington, Virginia 22217	2
ONR Branch Office Attn: Dr. George Sandoz 536 S. Clark Street Chicago, Illinois 60605	1
ONR Area Office Attn: Scientific Dept. 715 Broadway New York, New York 10003	1
ONR Western Regional Office 1030 East Green Street Pasadena, California 91106	1
ONR Eastern/Central Regional Office Attn: Dr. L. H. Peebles Building 114, Section D 666 Summer Street Boston, Massachusetts 02210	1
Director, Naval Research Laboratory Attn: Code 6100 Washington, D.C. 20390	1
The Assistant Secretary of the Navy (RE&S) Department of the Navy Room 4E736, Pentagon Washington, D.C. 20350	1
Commander, Naval Air Systems Command Attn: Code 310C (H. Rosenwasser) Department of the Navy Washington, D.C. 20360	1
Defense Technical Information Center Building 5, Cameron Station Alexandria, Virginia 22314	12
Dr. Fred Saalfeld Chemistry Division, Code 6100 Naval Research Laboratory Washington, D.C. 20375	1
Dr. Rudolph J. Marcus Office of Naval Research Scientific Liaison Group - Amer. Embassy A.P.O. San Francisco, CA. 96503	1
U.S. Army Research Office Attn: CRD-AA-IP P.O. Box 1211 Research Triangle Park, N.C. 27709	1
Naval Ocean Systems Center Attn: Mr. Joe McCartney San Diego, California 92152	1
Naval Weapons Center Attn: Dr. A. B. Amster, Chemistry Division China Lake, California 93555	1
Naval Civil Engineering Laboratory Attn: Dr. R. W. Drisko Port Hueneme, California 93401	1
Department of Physics & Chemistry Naval Postgraduate School Monterey, California 93940	1
Dr. A. L. Slafkosky Scientific Advisor Commandant of the Marine Corps (Code RD-1) Washington, D.C. 20380	1
Office of Naval Research Attn: Dr. Richard S. Miller 800 N. Quincy Street Arlington, Virginia 22217	1
Naval Ship Research and Development Center Attn: Dr. G. Bosmajian, Applied Chemistry Division Annapolis, Maryland 21401	1
Naval Ocean Systems Center Attn: Dr. S. Yamamoto, Marine Sciences Division San Diego, California 91232	1
Mr. John Boyle Materials Branch Naval Ship Engineering Center Philadelphia, Pennsylvania 19112	1
Mr. James Kelley DTNSRDC Code 2803 Annapolis, Maryland 21402	1

TECHNICAL REPORT DISTRIBUTION LIST, 051C

	No. Copies
Dr. M. B. Denton Department of Chemistry University of Arizona Tucson, Arizona 85721	1
Dr. R. A. Osteryoung Department of Chemistry State University of New York at Buffalo Buffalo, New York 14214	1
Dr. B. R. Kowalski Department of Chemistry University of Washington Seattle, Washington 98105	1
Dr. S. P. Perone Department of Chemistry Purdue University Lafayette, Indiana 47907	1
Dr. D. L. Venezky Naval Research Laboratory Code 6130 Washington, D.C. 20375	1
Dr. H. Freiser Department of Chemistry University of Arizona Tucson, Arizona 85721	
Dr. Fred Saalfeld Naval Research Laboratory Code 6110 Washington, D.C. 20375	1
Dr. H. Chernoff Department of Mathematics Massachusetts Institute of Technology Cambridge, Massachusetts 02139	1
Dr. K. Wilson Department of Chemistry University of California, San Diego La Jolla, California	1
Dr. A. Zirino Naval Undersea Center San Diego, California 92132	1
Dr. John Duffin United States Naval Postgraduate School Monterey, California 93940	1
Dr. G. M. Hieftje Department of Chemistry Indiana University Bloomington, Indiana 47401	1
Dr. Victor L. Rehn Naval Weapons Center Code 3813 China Lake, California 93555	
Dr. Christie G. Enke Michigan State University Department of Chemistry East Lansing, Michigan 48824	1
Dr. Kent Eisentraut, MBT Air Force Materials Laboratory Wright-Patterson AFB, Ohio 45433	1
Walter G. Cox, Code 3632 Naval Underwater Systems Center Building 148 Newport, Rhode Island 02840	1
Professor Isiah M. Warner Texas A&M University Department of Chemistry College Station, Texas 77840	1
Professor George H. Morrison Cornell University Department of Chemisty Ithaca, New York 14853	1
Professor J. Janata Department of Bioengineering University of Utah Salt Lake City, Utah 84112	1
Dr. Carl Heller Naval Weapons Center China Lake, California 93555	1
Dr. L. Jarvis Code 6100 Naval Research Laboratory Washington, D. C. 20375	1

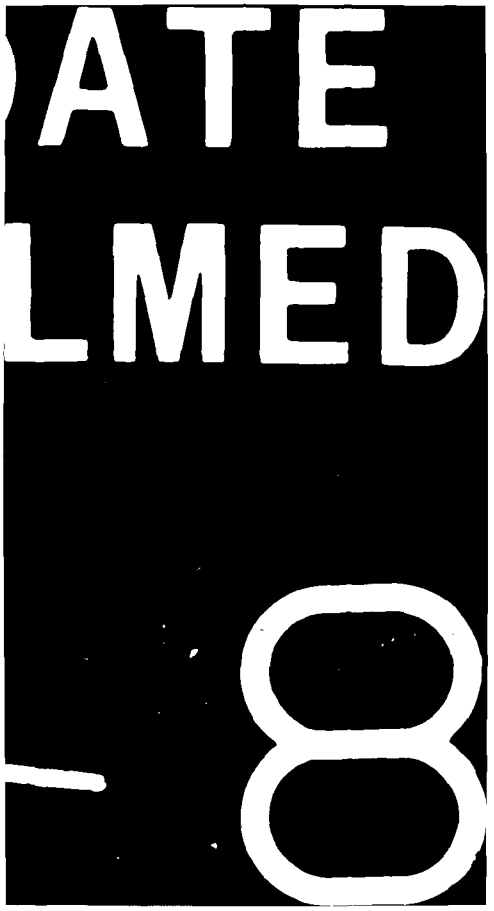
ATE
LMED
8